The Astrophysical Journal, 974:92 (14pp), 2024 October 10 https://doi.org/10.3847/1538-4357/ad66cf

The JWST UNCOVER Treasury Survey: Ultradeep NIRSpec and NIRCam Observations before the Epoch of Reionization

Rachel Bezanson[1], Ivo Labbe[2], Katherine E. Whitaker[3,4], Joel Leja[5,6,7], Sedona H. Price[1], Marijn Franx[8], Gabriel Brammer[4], Danilo Marchesini[9], Adi Zitrin[10], Bingjie Wang (王冰洁)[5,6,7], John R. Weaver[3], Lukas J. Furtak[10], Hakim Atek[11], Dan Coe[12,13,14], Sam E. Cutler[3], Pratika Dayal[15], Pieter van Dokkum[16], Robert Feldmann[17], Natascha M. Förster Schreiber[18], Seiji Fujimoto[19,35], Marla Geha[16], Karl Glazebrook[2], Anna de Graaff[20], Jenny E. Greene[21], Stéphanie Juneau[22], Susan Kassin[12], Mariska Kriek[8], Gourav Khullar[1], Michael Maseda[23], Lamiya A. Mowla[24], Adam Muzzin[25], Themiya Nanayakkara[2], Erica J. Nelson[26], Pascal A. Oesch[4,27], Camilla Pacifici[12], Richard Pan[9], Casey Papovich[28,29], David J. Setton[1], Alice E. Shapley[30], Renske Smit[31], Mauro Stefanon[32,33], Edward N. Taylor[2], and Christina C. Williams[22,34]

[1] Department of Physics and Astronomy and PITT PACC, University of Pittsburgh, Pittsburgh, PA 15260, USA
[2] Centre for Astrophysics and Supercomputing, Swinburne University of Technology, Melbourne, VIC 3122, Australia
[3] Department of Astronomy, University of Massachusetts, Amherst, MA 01003, USA
[4] Cosmic Dawn Center (DAWN), Niels Bohr Institute, University of Copenhagen, Jagtvej 128, København N, DK-2200, Denmark
[5] Department of Astronomy & Astrophysics, The Pennsylvania State University, University Park, PA 16802, USA
[6] Institute for Computational & Data Sciences, The Pennsylvania State University, University Park, PA 16802, USA
[7] Institute for Gravitation and the Cosmos, The Pennsylvania State University, University Park, PA 16802, USA
[8] Leiden Observatory, Leiden University, P.O.Box 9513, NL-2300 AA Leiden, The Netherlands
[9] Department of Physics and Astronomy, Tufts University, 574 Boston Avenue, Medford, MA 02155, USA
[10] Physics Department, Ben-Gurion University of the Negev, P.O. Box 653, Beer-Sheva 8410501, Israel
[11] Institut d'Astrophysique de Paris, CNRS, Sorbonne Université, 98bis Boulevard Arago, 75014, Paris, France
[12] Space Telescope Science Institute (STScI), 3700 San Martin Drive, Baltimore, MD 21218, USA
[13] Association of Universities for Research in Astronomy (AURA), Inc. for the European Space Agency (ESA), USA
[14] Center for Astrophysical Sciences, Department of Physics and Astronomy, The Johns Hopkins University, 3400 N Charles Street, Baltimore, MD 21218, USA
[15] Kapteyn Astronomical Institute, University of Groningen, P.O. Box 800, 9700 AV Groningen, The Netherlands
[16] Department of Astronomy, Yale University, New Haven, CT 06511, USA
[17] Institute for Computational Science, University of Zurich, Winterhurerstrasse 190, CH-8006 Zurich, Switzerland
[18] Max-Planck-Institut für extraterrestrische Physik, Gießenbachstraße 1, 85748 Garching, Germany
[19] Department of Astronomy, The University of Texas at Austin, Austin, TX 78712, USA
[20] Max-Planck-Institut für Astronomie, Königstuhl 17, D-69117, Heidelberg, Germany
[21] Department of Astrophysical Sciences, 4 Ivy Lane, Princeton University, Princeton, NJ 08544, USA
[22] NSF's National Optical-Infrared Astronomy Research Laboratory, 950 N. Cherry Avenue, Tucson, AZ 85719, USA
[23] Department of Astronomy, University of Wisconsin-Madison, 475 N. Charter Street, Madison, WI 53706, USA
[24] Dunlap Institute for Astronomy and Astrophysics, 50 Street George Street, Toronto, ON M5S 3H4, Canada
[25] Department of Physics and Astronomy, York University, 4700 Keele Street, Toronto, ON MJ3 1P3, Canada
[26] Department for Astrophysical and Planetary Science, University of Colorado, Boulder, CO 80309, USA
[27] Department of Astronomy, University of Geneva, Chemin Pegasi 51, 1290 Versoix, Switzerland
[28] Department of Physics and Astronomy, Texas A&M University, College Station, TX, 77843-4242, USA
[29] George P. and Cynthia Woods Mitchell Institute for Fundamental Physics and Astronomy, Texas A&M University, College Station, TX, 77843-4242, USA
[30] Physics & Astronomy Department, University of California Los Angeles, 430 Portola Plaza, Los Angeles, CA 90095, USA
[31] Astrophysics Research Institute, Liverpool John Moores University, 146 Brownlow Hill, Liverpool, L3 5RF, UK
[32] Departament d'Astronomia i Astrofisica, Universitat de Valencia, C. Dr. Moliner 50, E-46100 Burjassot, Valencia, Spain
[33] Unidad Asociada CSIC "Grupo de Astrofisica Extragalactica y Cosmologi" (Instituto de Fisica de Cantabria—Universitat de Valencia), Spain
[34] Steward Observatory, University of Arizona, 933 North Cherry Avenue, Tucson, AZ 85721, USA
Received 2022 December 7; revised 2024 June 28; accepted 2024 July 22; published 2024 October 7

Abstract

In this paper we describe the survey design for the Ultradeep NIRSpec and NIRCam Observations before the Epoch of Reionization (UNCOVER) Cycle 1 JWST Treasury program, which executed its early imaging component in 2022 November. The UNCOVER survey includes ultradeep (∼29–30AB) imaging of ∼45 arcmin^2 on and around the well-studied A2744 galaxy cluster at $z = 0.308$ and will follow up ∼500 galaxies with extremely deep low-resolution spectroscopy with the NIRSpec/PRISM during the summer of 2023, with repeat visits in summer 2024. We describe the science goals, survey design, target selection, and planned data releases. We also present and characterize the depths of the first NIRCam imaging mosaic, highlighting previously unparalleled resolved and ultradeep 2–4 μm imaging of known objects in the field. The UNCOVER primary NIRCam mosaic spans 28.8 arcmin^2 in seven filters (F115W, F150W, F200W, F277W, F356W, F410M, and F444W) and 16.8 arcmin^2 in our NIRISS parallel (F115W, F150W, F200W, F356W, and F444W). To maximize early

[35] Hubble Fellow.

community use of the Treasury data set, we publicly release the full reduced mosaics of public JWST imaging including 45 arcmin^2 NIRCam and 17 arcmin^2 NIRISS mosaics on and around the A2744 cluster, including the Hubble Frontier Field primary and parallel footprints.

Unified Astronomy Thesaurus concepts: James Webb Space Telescope (2291); Redshift surveys (1378); Galaxy evolution (594); Galaxy formation (595); Observational astronomy (1145); Abell clusters (9); High-redshift galaxies (734); Galaxies (573)

1. Introduction

A lasting legacy of the Hubble Space Telescope (HST) and Spitzer Space Telescope is the discovery and characterization of galaxies to $z \sim 11$, looking back 97% of the time to the Big Bang (e.g., Coe et al. 2013; Oesch et al. 2016). Extragalactic deep fields with Hubble imaging and grism spectroscopy to $\sim$1.6 μm have provided a reasonably complete census of the cosmic star formation history (e.g., Madau & Dickinson 2014; Finkelstein et al. 2015; Oesch et al. 2018; Bouwens et al. 2022b), and combined with Spitzer imaging, constraints on the mass functions of galaxies since $z = 3$ (e.g., Duncan et al. 2014; Grazian et al. 2015; Song et al. 2016; Bhatawdekar et al. 2019; Kikuchihara et al. 2020; Leja et al. 2020; Furtak et al. 2021; Stefanon et al. 2021). However, despite 10,000 HST orbits and tens of thousands of hours of Spitzer observations, our picture of the Universe remains highly incomplete due to reliance on HST selection (rest-frame UV at $z > 4$). This means we were biased toward the youngest, least dusty galaxies, and had been unable to study the first galaxies at $z \gtrsim 12$. Understanding these first galaxies is crucial since they mark the start of the process of cosmic reionization and are the first sources of metals in the Universe (e.g., Dayal & Ferrara 2018).

The JWST was specifically designed to address these limitations by providing high-throughput, sensitive imaging and spectroscopy at 1–5 μm with the NIRCam (Rieke et al. 2003, 2005, 2023), NIRISS (Doyon et al. 2012) and NIRSpec instruments (Jakobsen et al. 2022; Böker et al. 2023; Rigby et al. 2023). These capabilities have begun to enable us to find galaxies deep into the Dark Ages ($z = 10$–20; e.g., Naidu et al. 2022a; Finkelstein et al. 2022; Adams et al. 2023; Atek et al. 2023; Donnan et al. 2023; Harikane et al. 2023), to directly study the faint galaxies responsible for reionizing the universe a few hundred million years later and identifying dusty and quiescent galaxies to low masses to redshift $z \sim 10$ (e.g., Naidu et al. 2022b; Carnall et al. 2022; Labbé et al. 2023; Nelson et al. 2023; Zavala et al. 2023). The intrinsically faintest galaxies can be reached with the aid of gravitational lensing. Observations with HST along gravitational lensing galaxy clusters (e.g., in the Hubble Frontier Fields, HFF; Lotz et al. 2017) have identified some exceptionally magnified individual objects (e.g., Zitrin et al. 2014; Kelly et al. 2015), increasing effective depths of, e.g., reionization-era UV luminosity functions by several magnitudes (e.g., Atek et al. 2018; Ishigaki et al. 2018; Bouwens et al. 2021, 2022a, 2022b; Kauffmann et al. 2022). However, at the faintest ends, these studies remain besieged by systematics.

It is in this context that the Ultradeep NIRSpec and NIRCam Observations before the Epoch of Reionization (UNCOVER) Treasury survey was designed (PIs: Labbé & Bezanson, JWST-GO#2561). UNCOVER targets the powerful lensing cluster A2744 and consists of two coordinated components executed in the same cycle. First, a deep NIRCam pre-imaging mosaic in seven filters for $\sim$4–6 hr per band, and second ultradeep 3–20 hr NIRSpec/PRISM low-resolution follow-up of NIRCam-detected high-redshift galaxies—each with NIRISS or NIRCam imaging parallels. The imaging and spectroscopy leverage the gravitational lensing boost to push beyond depths achievable in blank fields. Perhaps the most exciting legacy is the potential to discover "unknown unknowns," objects we have not yet imagined or anticipated. The advance in sensitivity, wavelength coverage, and spectral resolution (in comparison to Spitzer imaging) is so great that we are almost guaranteed to run into surprises. Covering ultradeep parameter space with imaging and spectroscopy early in JWST's mission helps to ensure ample time for follow-up studies in future cycles.

In Figure 1 we show the full area of the UNCOVER survey (purple star) in the context of other HST (blue circles) and JWST Cycle 1 extragalactic deep fields (red squares). UNCOVER is more than a magnitude deeper than other wide-field surveys. Only the ultradeep NGDEEP (Bagley et al. 2024) survey and Guaranteed Time Observation (GTO) ultradeep field (JADES; PI: Eisenstein, JWST-GTO1180) probe beyond UNCOVER, and these depths do not account for the effects of gravitational lensing. The A2744 lensing cluster boosts the intrinsic limits of UNCOVER, sacrificing area (see arrows indicating the effect of a factor of $\sim$5 magnification in cluster fields) to make it the deepest extragalactic field in Cycle 1 of JWST observations. Furthermore, UNCOVER is the only GO data set that collected deep spectroscopic follow-up of JWST-selected objects with no proprietary time in Cycle 1.

The outline of this paper is as follows. The survey design of the UNCOVER program is presented in Section 2. This paper includes the public release of early reduced mosaics of NIRCam cluster pre-imaging and NIRISS parallel imaging, described in Section 3. We summarize the science cases that will be enabled by the UNCOVER data set in Section 4. Finally, we summarize the prospects of the UNCOVER survey in Section 5. Throughout this paper, we adopt a standard Lambda cold dark matter (ΛCDM) cosmology with $H_0 = 70$ km s^{-1}Mpc^{-1}, $\Omega_M = 0.3$, and $\Omega_\Lambda = 0.7$.

2. Survey Design

2.1. Observational Strategy

The first UNCOVER data consist of deep (4–6 hr per filter) NIRCam pre-imaging on the A2744 cluster to $\sim$29.5–30 AB magnitude in seven filters, collected in 2022 November. Nine months later 2023 July/August we targeted sources detected in NIRCam with ultradeep 19 hr NIRSpec/PRISM low-resolution spectroscopy. (Due to technical issues, a fraction of NIRSpec observations will be repeated in 2024 July/August.) Both sets of observations include deep parallel imaging (in NIRISS and NIRCam, respectively), to increase the area for deep photometric studies of high-redshift galaxies at mild (1.1–1.3×) lensing magnification. The footprints of these components are shown in Figure 2 (left panel) and reproduced along with

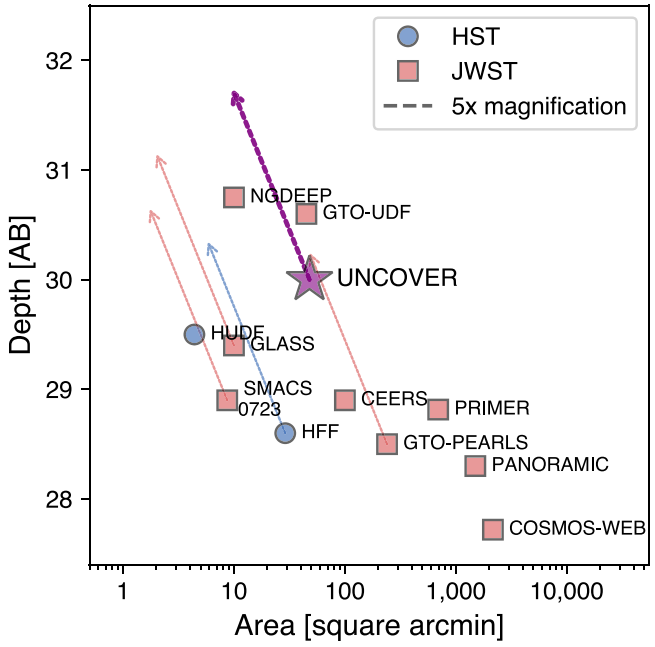

Figure 1. The UNCOVER combined imaging (purple star) probes a unique regime in the context of HST extragalactic ultradeep fields (blue circles) and JWST Cycle 1 imaging surveys (red squares); without lensing it probes deeper than previous HST surveys and wide-field programs. Gravitational lensing (approximate lensing vectors indicated by dashed arrows) from the A2744 allows UNCOVER imaging to probe the intrinsically faintest objects of any JWST project in Cycle 1. We note that lensing vectors are approximate, as the UNCOVER survey includes lensed and unlensed areas of A2744.

ancillary data from HST and the Very Large Telescope (VLT) Multi-Unit Spectroscopic Explorer (MUSE; center panel), as well as other Cycle 1 JWST data (right panel).

2.2. Field Selection

A2744 is one of the most powerful known gravitational lensing clusters, with a large area of high magnification ($\mu > 2$, 4, 10 over >17, 7, 2 arcmin^2), because the cluster itself consists of several merging subclusters, or massive subclumps (e.g., Merten et al. 2011; Richard et al. 2014; Jauzac et al. 2015; Wang et al. 2015; Diego et al. 2016; Kawamata et al. 2016). The full complex stretches toward the northwest of the HFF cluster pointing. The NIRCam footprint is designed to span the $\mu > 2$ magnification contour (see Figure 3). The cluster contains many HST-detected $6 < z < 10$ galaxies, underscoring its efficacy. The field has excellent roll angle visibility for JWST and a low infrared background (ideal for deep background-limited observations). The observing windows (2022 November for the imaging and expected 2023 July for spectroscopy) benefit from the lowest possible backgrounds in Cycle 1. The field also contains some of the best complementary multiwavelength data (including deep 29AB HST Advanced Camera for Surveys, ACS, optical data) and is accessible by the Atacama Large Millimeter/submillimeter Array (ALMA); we summarize ancillary data sets in Section 2.5.

2.3. Deep NIRCam and NIRISS Imaging

The UNCOVER survey imaging includes deep primary NIRCam imaging on the extended cluster and NIRISS and NIRCam parallel imaging in the outskirts. In this section, we describe the NIRCam primary field cluster pre-imaging mosaic and the NIRISS parallel.

The NIRCam mosaic is designed to maximize the number of detected $z > 10$ galaxies. This was done by forward-modeling the theoretical luminosity functions of Mason et al. (2015) and from the `DELPHI` model (Dayal et al. 2014, 2022) using the CATS v4.1 lens model of A2744 (Jauzac et al. 2015) to predict the number of $6 < z < 16$ galaxies to our detection limit. The number of $z > 10$ galaxies is maximized by a four-pointing gap-filled NIRCam mosaic. Our expected 5σ depths of $\sim$30 AB (given $\sim$4 hr of exposure in F200W and $\sim$6 hr in F115W, JWST ETC 2.0; see Table 1) correspond to $M_{\rm UV} = -14.0$ at $z = 6$–7 with <3 mag of lensing (where models are considered more robust; e.g., Livermore et al. 2017; Atek et al. 2018; Bouwens et al. 2021). The dominant uncertainty in expected numbers is the difference between theoretical models, which can differ by factors of >10 at $z > 10$ (e.g., Oesch et al. 2018; Finkelstein et al. 2023), with a smaller contribution from cosmic variance ranging from 10% to 40% at $z = 7$–10 (e.g., Ucci et al. 2021). These depths compare favorably to those achieved in our final mosaic (see Table 1).

NIRCam pre-imaging is taken with a four-pointing mosaic and an eight-pointing INTRAMODULEX dither pattern for 3.7–6 hr, using six broadband filters (F115W, F150W, F200W, F277W, F356W, and F444W). A medium-band filter F410M is added, to improve diagnostics of emission lines and improve photometric redshifts and stellar masses of high-z galaxies (Kauffmann et al. 2020; Roberts-Borsani et al. 2021; Labbé et al. 2023). We note that the same extended mosaic was followed up with JWST/NIRCam imaging as part of programs JWST-GO-4111 (PI: Suess) and JWST-GO-3516 (PIs: Matthee and Naidu), which added bluer broadband filters (F070W and F090W) and all remaining medium-band filters. Exposure times and approximate imaging depths are listed in Table 1 and filter curves are shown in Figure 4. In that Figure, we show representative SEDs generated using `Bagpipes` (Carnall et al. 2018) with the NIRCam primary filters. We show delayed tau models ($\log M_\star/M_\odot = 9.2$) in the top four panels (100 Myr old in purple for the earliest galaxies, 300 Myr old in blue for the $z \sim 6$–8, $A_V = 3$ dusty galaxies in orange, and 500 Myr old quiescent galaxies in red). NIRISS parallel imaging includes only F115W, F150W, F200W, F356W, and F444W broad bands. This field lacks some filters with respect to the NIRCam primary imaging as NIRISS lacks NIRCam's dichroic. The NIRISS parallel imaging fortuitously overlaps with the 42-orbit 29AB F814W HFF A2744 ACS parallel field, obviating the need for additional optical data. The first NIRCam/ NIRISS imaging data were collected on 2022 November 2, 4, 7, and 15. The final visit was a repeat observation of visit 1:1, which initially failed in guide star acquisition (on 2022 October 31). The new visit 3:1 was observed at a slightly different angle (V3PA $= 45.00°$ relative to V3PA $= 41.3588°$ for the other three visits) and higher background level to facilitate rapid rescheduling. This results in a slightly askew mosaic footprint, but image depths and footprint are minimally impacted by this change.

In parallel to the follow-up NIRSpec observations, a second imaging parallel field will be taken with NIRCam using a more expanded set of seven broadband filters (F090W, F115W, F150W, F200W, F277W, F356W, F444W) and two medium-band filters (F335M and F410M) with total exposure times of 2.6–5.3 hr. The expanded filter set mitigates the lack of optical

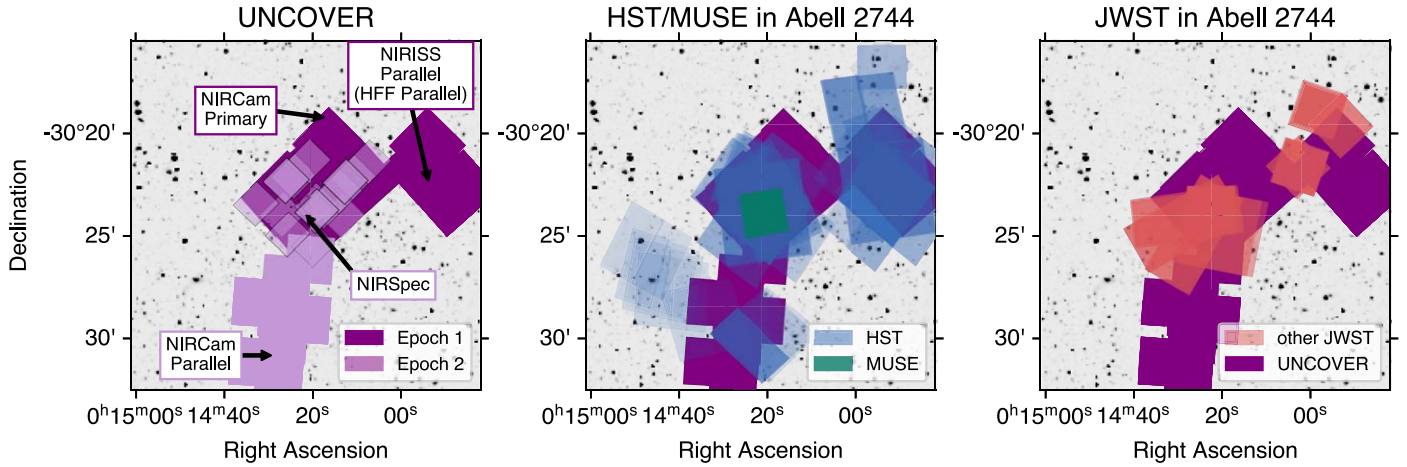

Figure 2. The A2744 cluster has extensive deep optical/NIR (HST and VLT/MUSE) and JWST coverage. The JWST/UNCOVER footprints (purple) along with HST imaging (blue) and VLT/MUSE deep data cube (green, center) and JWST Cycle 1 imaging and spectroscopy (red, right) against imaging from the Legacy Imaging survey (Dey et al. 2019). An updated version with Cycle 2 JWST programs can be found in Suess et al. (2024). In the left panel, we highlight the detailed layout of the UNCOVER data set, differentiating between the first epoch (dark purple, NIRCam primary imaging and NIRISS parallel imaging) and second epoch (planned NIRSpec spectroscopy and NIRCam parallel imaging, light purple). The NIRCam mosaic is designed to match the $\mu = 2$ magnification curve (see Figure 3). The footprints of the NIRSpec spectroscopy are provisional and subject to target selection.

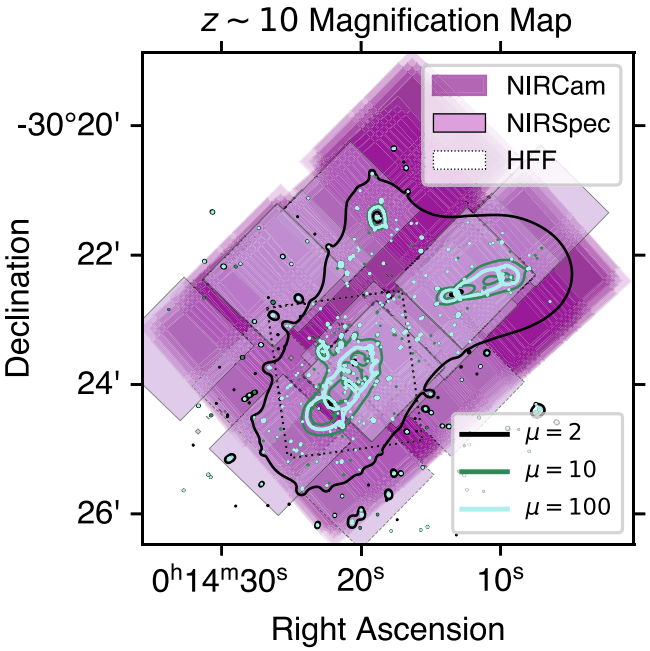

Figure 3. Gravitational lensing magnification contours in A2744 are extremely extended, due to the complex structure of the multiple cluster cores. The above curves are taken from the UNCOVER-based lensing model at $z \sim 10$ (Furtak et al. 2023c). The UNCOVER NIRCam mosaic (dark purple) spans the $\mu = 2$ curve, which is significantly larger than the HFF (black dashed outline). By extending to the northern subclumps the UNCOVER mosaic enables a more detailed mapping of that region.

Table 1
UNCOVER Imaging

Instrument	Filter	Exposure	Dates	5σ Depth	ETC
NIRCam	F115W	6.0 hr	2022 Nov 2, 4, 7, 15	30.05	29.9
(Primary)	F150W	6.0 hr		30.18	30.1
	F200W	3.7 hr		30.12	30.0
	F277W	3.7 hr		29.75	29.5
	F356W	3.7 hr		29.79	29.5
	F410M	3.7 hr		29.03	28.8
	F444W	4.6 hr		29.25	29.2
NIRISS	F115W	3.7 hr	(See primary)	30.19	30.1
(Parallel)	F150W	3.7 hr		30.13	30.2
	F200W	3.7 hr		30.25	30.2
	F356W	2.1 hr		29.40	29.2
	F444W	2.1 hr		28.8	28.6
NIRCam	F090W	5.3 hr	2023 Jul/**Aug**	⋯	29.7
(Parallel)	F115W	5.3 hr		⋯	29.8
	F150W	5.3 hr		⋯	30.0
	F200W	2.6 hr		⋯	29.8
	F277W	2.6 hr		⋯	29.3
	F335M	2.6 hr		⋯	29.0
	F356W	2.6 hr		⋯	29.3
	F410M	2.6 hr		⋯	28.6
	F444W	5.3 hr		⋯	29.2

Note. Imaging depths in the NIRISS/NIRCam mosaics are calculated using 0.″08 radius apertures in the short-wavelength bands, 0.″16 radius apertures in the long-wavelength bands, based on the noise properties inferred from the weight maps and corrected to total assuming point sources. The depths correspond to the two-visit depth regions of the mosaic. ETC values correspond to S/N = 5 point source depths using JWST ETC v2.0. We refer the reader to Weaver et al. (2024) for a more detailed discussion of the effective depths of our photometric catalogs and Price et al. (2024) for the NIRCam parallel imaging.

data in that pointing. The NIRCam parallel observations are taken with the NIRSpec/PRISM in MOS mode with a 3-POINT-WITH-NIRCam-SIZE2 dither pattern and a three-slitlet nod pattern.

2.4. Scheduled NIRSpec/PRISM Spectroscopic Follow-up

The spectroscopic component of the UNCOVER survey was completed in 2023 July/August, aside from a failed visit that was impacted by an electrical short. We describe the final spectroscopic program design and observational strategy in Price et al. (2024). These spectra are designed to be ultradeep, using the low-resolution ($R \sim 30$–300) PRISM mode to provide the deepest continuum depths and widest wavelength coverage (0.6–5.3 μm). A primary goal of UNCOVER is to detect continuum flux and to measure continuum redshifts of any faint

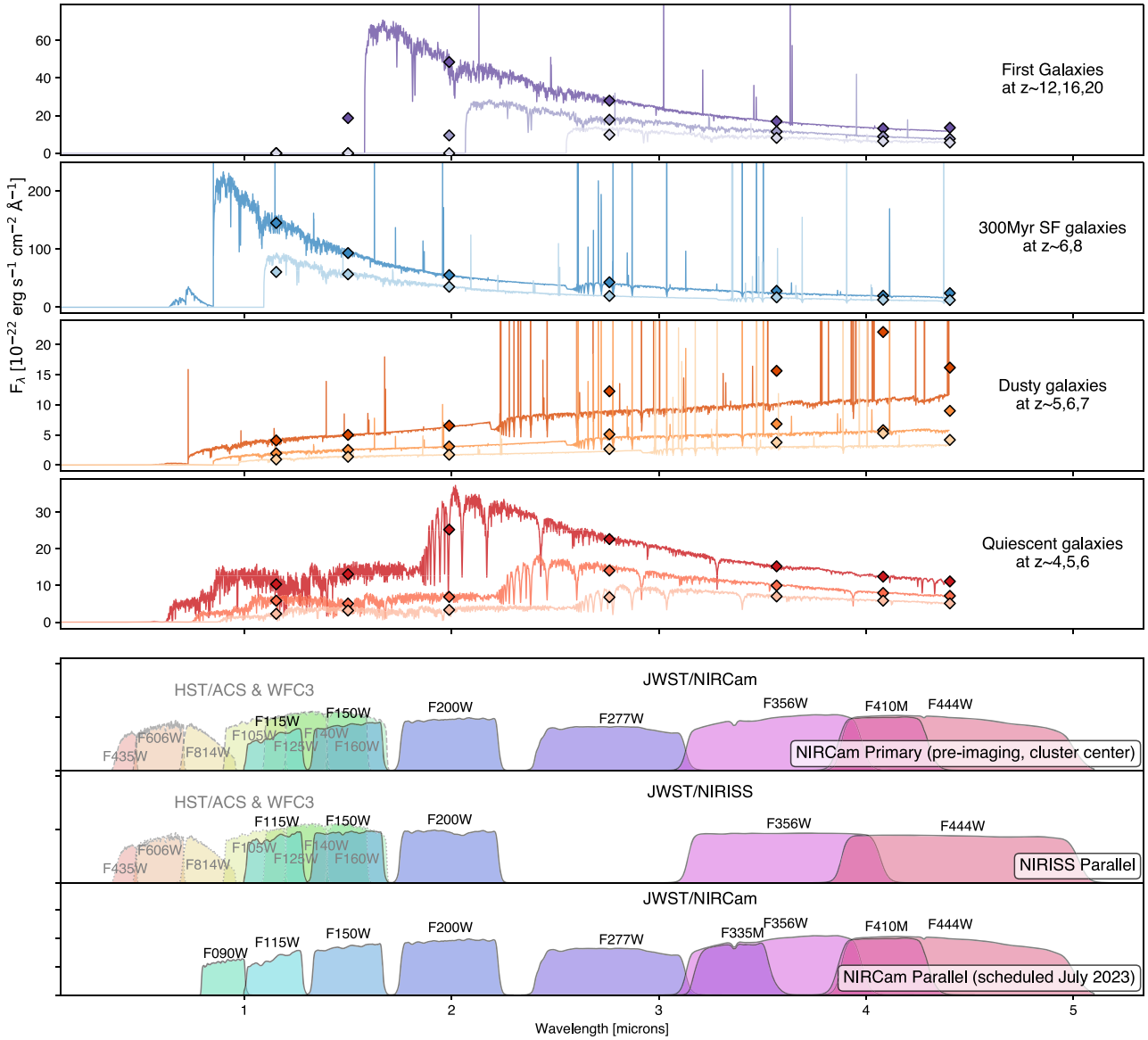

Figure 4. Top rows: model SEDs for four key galaxy types. Bottom rows: filter curves for deep HST and JWST imaging in the three UNCOVER imaging fields. HST imaging (ACS and WFC3) from the HFF program overlaps with the A2744 cluster center (UNCOVER NIRCam primary, top row) and the HFF parallel imaging overlaps with the UNCOVER NIRISS parallel (middle panel). The NIRCam parallel lacks deep optical imaging from HST but includes F090W and two medium-band filters (F335M and F410M).

high-redshift object detected securely with NIRCam (10σ, $\sim$29 AB). This requires a signal-to-noise ratio of SNR = 3 per resolution element at 1.5 μm, which can be reached in $\sim$20 hr integration. For galaxies with strong emission lines, we can measure redshifts and emission line strengths to $\sim$30 AB if $EW_{obs} > 600$ Å corresponding to, e.g., rest-frame $EW_0(H\alpha,0) > 100$ Å at $z = 6$ or $EW_0([O\,III]_{5007}) > 60$ Å at $z = 9$. Typical galaxies at these redshifts have $>5\times$ stronger emission lines (e.g., Stark 2012; Labbé et al. 2013; Smit et al. 2014; Stefanon et al. 2021, 2022; Williams et al. 2023); we expect to measure redshifts for the vast majority of targets found by NIRCam.

The broad wavelength coverage spans critical spectral features for all potential targets. Simulated spectra for a number of targets are shown in Figure 5. From Cosmic Dawn through reionization, our PRISM spectra will probe UV flux and Lyα and will include rest-frame optical emission lines (including Hα and [N II] below $z \sim 7$). Deep exposure times probe rest-optical emission lines to measure low-level star formation, dust attenuation, and active galactic nucleus (AGN) activity in dusty galaxies. Finally, the Balmer absorption features and Balmer/4000 Å breaks can be clearly detected for even the most distant quiescent candidates. We include a similar figure with real spectra in Price et al. (2024).

Our planned spectroscopic targets will be roughly prioritized according to scientific value and rarity:

1. Any $z > 12$ candidates.
2. $z > 9$ galaxies prioritized by brightness.
3. Pop III candidate sources.
4. Faint highly magnified $6 < z < 7$ galaxies.
5. Quiescent galaxies $z > 4$.
6. $z > 6$ AGN.
7. Dusty galaxies $z > 4$.

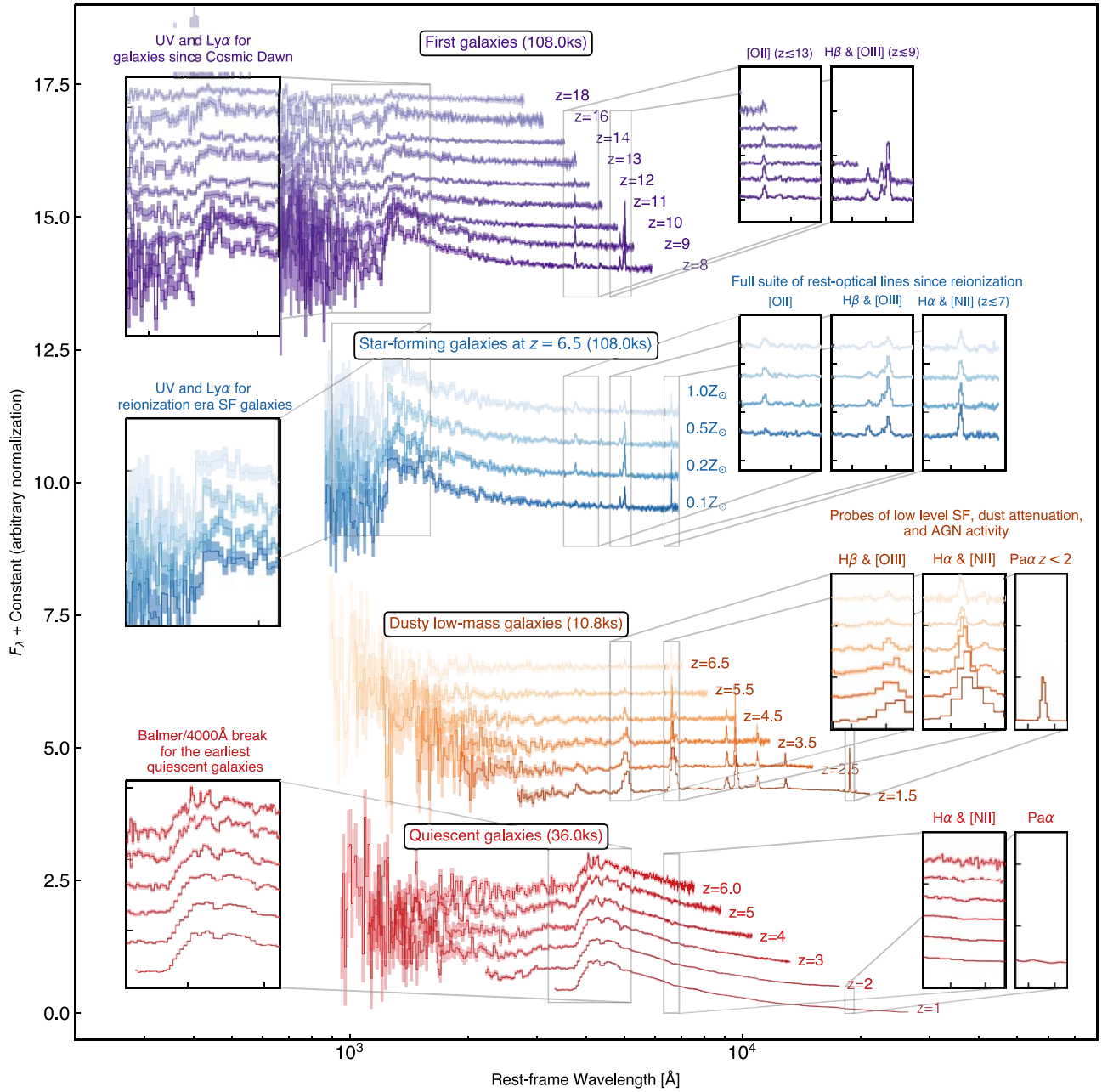

Figure 5. Simulated PRISM spectra of a variety of UNCOVER targets, with similar SEDs to those presented in Figure 4, with total exposure times ranging from 2.7 to 17.4 hr. The wide wavelength coverage (0.6–5.3 μm) of the NIRSpec/PRISM spectra catch critical spectroscopic features, with a resolution up to $R \sim 300$ at the red end. Ultradeep exposures probe the continuum flux for nearly all sources and the multiple mask designs provide spectra for ∼500–1000 targets.

8. Low-mass quiescent galaxies at $1 < z < 6$.
9. Any unusual or unexpected sources.
10. Extreme emission line galaxies.
11. Mass-selected galaxies sampled in bins of mass and redshift.

We estimate that we can accommodate ∼15–20 sources to our full depth of 17.4 hr. Other sources require less exposure time. This is accomplished by switching individual sources in and out of overlapping micro-shutter array (MSA) designs (described below). Approximate numbers for key target classes are included in Table 2, estimated from Williams et al. (2018) and Mason et al. (2015) models. The full implementation of this MSA design will be presented in Price et al. (2024).

The total NIRSpec integration times are designed to be split up into seven partially overlapping dithered sequences of 2.7–4 hr each. We therefore designed seven masks with exposure times ranging from 2.7 to 17.4 hr, repeating the high-priority objects. Each of our seven MSA configurations is designed in an iterative manner, with the possibility of keeping objects on multiple masks. Observations will follow a three-point dither pattern (3-POINT-WITH-NIRCAM-SIZE2). We adopt the NRSIRS2 readout pattern, averaging five frames into groups to optimize the noise characteristics. Given the high target density of some lower-priority targets (e.g., there will be 1000 s of high-z emission line galaxies), we expect to fill each mask with ∼100 targets for a total of ∼500 unique sources in the spectroscopic sample.

Table 2
Predicted Galaxy Counts in UNCOVER

Category	Lensed (Cluster)	Parallel
$z \gtrsim 12$ candidates	36	9
$9 < z < 12$ candidates	∼100 s	∼50
$6 \lesssim z \lesssim 7$ galaxies	∼1500	∼1500
$z > 1$ Dusty star-forming galaxies	∼50	∼150
$z > 3$ Quiescent galaxies	>6	>10
$1 < z < 3$ Quiescent galaxies	>20	>60

Note. The photometric data set inevitably yielded other extraordinary targets that have been included in the MSA designs including, but not limited to: black hole seeds, extremely lensed galaxies, and stars. All numbers are rough estimates derived from the JAdes extraGalactic Ultradeep Artificial Realizations mock catalog (Williams et al. 2018) below $z < 6$ and at higher redshifts from the Mason et al. (2015) model. Spectroscopic follow-up prioritizes highly lensed or otherwise remarkable objects.

Slit loss through the MSA will be significant and wavelength dependent due to variations in the point-spread function, complicating precise flux calibration. However, because the UNCOVER program includes multiband NIRCam pre-imaging, our team is well-positioned to perform corrections for these wavelength-dependent aperture effects, leveraging flexible, spatially resolved galaxy models (Leja et al. 2021).

2.5. Ancillary Data Sets in A2744

A2744 has been targeted by a multitude of HST imaging, e.g., through the HFF program (Lotz et al. 2017) and the HST/BUFFALO survey (Steinhardt et al. 2020), which we enumerate along with a variety of other ancillary data sets in Table 3. HST/ACS imaging in the cluster center was taken by Program #11689 (PI: Dupke) and #13386 (PI: Rodney) and HST/WFC3 observations were collected through Program #13495 (PI: Lotz). In the HFF parallel (UNCOVER NIRISS parallel), HST/ACS imaging was taken by Programs #13386 (PI: Rodney), #13495 (PI: Lotz), and #13389 (PI: Siana) and HST/WFC3 imaging in that field was taken again by the HFF program (#13495, PI: Lotz). Although these deep HST observations were limited to the field of view of individual ACS or WFC3 pointings, the footprints were expanded by the BUFFALO survey (Program #15117, PI: Steinhardt; Steinhardt et al. 2020), which expands the main cluster and parallel footprints by a factor of four. Recently, the deep optical coverage was expanded by Program #17231 (PI: Treu; Paris et al. 2023). Among other things, this wide area enables improved lens models.

In addition, the A2744 cluster has been targeted by ground-based imaging and spectroscopic programs. One such rich data set is provided by deep VLT/MUSE observations. This mosaic of MUSE pointings covers $2' \times 2'$ and yields untargeted spectroscopic redshifts for 514 galaxies (Mahler et al. 2018). These spectroscopic redshifts contribute to improved lensing models, especially for multiply imaged systems. Mahler et al. (2018) suggest that this improvement is approximately a factor of ∼2.5. Although Spitzer imaging in A2744 is largely superseded by novel JWST imaging from the UNCOVER survey, the field has also been observed in the X-ray for 110 ks by XMM-Newton (#074385010, PI: Kneib), 75 ks with Suzaku (Eckert et al. 2016), and Chandra (#23700107, PI Bogdan). Deep ground-based optical imaging exists from Subaru/Suprime-Cam in B, R_C, i', and z' (Medezinski et al. 2016). ALMA observations of the A2744 cluster include 1.1 mm imaging of the cluster through the HFF–ALMA program (González-López et al. 2017) and a 15 GHz wide spectral scan at 1.2 mm through the ALMA lensing cluster survey (Kohno 2019).

Already in the first cycle of JWST observations, several other programs targeted A2744. First, the Early Release Science (ERS) GLASS-JWST program (Treu et al. 2022, PI: Treu) targets the cluster center with deep targeted NIRSpec spectroscopy and NIRISS imaging and untargeted spectroscopy and obtains NIRCam parallel imaging in the cluster outskirts in the following broadband filters (F090W, F115W, F150W, F200W, F277W, F356W, F444W). For details about that program, the reader is referred to the survey design paper (Treu et al. 2022). All data from the GLASS-JWST are available with no proprietary period. Additionally, A2744 will be observed with NIRCam imaging as part of the JWST GTO Prime Extragalactic Areas for Reionization and Lensing Science (PEARLS) Program 1176 (PI: Windhorst), including ∼2 hr depth observations in F090W, F115W, F150W, F200W, F277W, F356W, F410M, and F444W to ∼28–29 AB 5σ limiting depths (Windhorst et al. 2023). Recently, a DDT program (#2756, PI: Chen) was approved to image and spectroscopically image a lensed, $z \sim 3.5$ supernova. That data set includes two epochs of NIRCam imaging (F115W, F150W, F200W, F277W, F356W, and F444W) and NIRSpec/PRISM spectra in the cluster center. A number of subsequent JWST programs have been completed in A2744; we refer the reader to Suess et al. (2024) for updated accounting and similar figures. Finally, $4' \times 6'$ of the cluster center (in the footprint of the UNCOVER NIRCam imaging) has been mapped by the Deep UNCOVER-ALMA Legacy High-z (DUALZ) survey ALMA Band 6 spectral scans (Fujimoto et al. 2023a).

2.6. Planned Data Release Schedule

While there is no proprietary period associated with the UNCOVER data set, our team is committed to the regular public release of reduced and high-level data products to maximize community use of this Treasury program. This paper represents the first of several data releases of the UNCOVER survey (Data Release 1, DR1); see the full anticipated release schedule in Table 4. We subsequently provided two incremental data releases (DR1 and DR2) prior to the JWST Cycle 2 proposal deadline, providing the community with an early photometric catalog based on archival HST imaging and NIRCam pre-imaging in the A2744 cluster (Weaver et al. 2024) in addition to a description and catalog of derived physical properties, including photometric redshifts and stellar population synthesis modeling with `Prospector` (Johnson et al. 2021; Wang et al. 2024). Additionally, our team has published lensing maps that have been updated with new JWST sources (Furtak et al. 2023c), magnification estimates and uncertainties from this model are included in photometric catalogs. We introduced a third data release to incorporate the additional broad and medium-band NIRCam imaging and NIRISS parallel fields along with all photometric data products (DR3; Suess et al. 2024). Within a year of our second epoch of data acquisition, we plan to publicly release reduced NIRSpec/PRISM spectra (Price et al. 2024) and lensing maps that have been updated with new JWST spectroscopic redshifts DR4.

Table 3
A2744 Ancillary Data

Target	Instrument	(Survey/) Program ID/PI	Notes/Depth
		JWST Cycle 1	
Cluster (HFF-core)	NIRSpec	GLASS/ERS-X1324/PI: Treu	52 ks
	NIRISS		35 ks
	NIRCam	DD-2756/PI: Chen	17 ks
	NIRSpec		
	NIRCam	GTO-PEARLS/GTO-1176/PI: Windhorst	12 ks
Field	NIRCam	GLASS/ERS-Treu/PI: Treu	30 ks, 50 ks
	F090W, F115W, F150W, F200W		
	F277W, F356W, F444W		
		HST	
Cluster (HFF-core)	ACS/F435W	#11689/PI: Dupke, #13386/PI: Rodney	18 orbits
	ACS/F606W		9 orbits
	ACS/F814W		41 orbits
	WFC3/F105W	#13495/PI: Lotz	24.5 orbits
	WFC3/F125W		12 orbits
	WFC3/F140W		10 orbits
	WFC3/F160W		24.5 orbits
Cluster (expanded)	ACS/F606W	BUFFALO, #15117, PI: Steinhardt	2/3 orbit
	ACS/F814W		4/3 orbit
	WFC3/F105W,F125W,F160W		2/3 orbit
Field	ACS/F435W	#13386/PI: Rodney, #13495/PI: Lotz, #13389/PI: Siana	6 orbits
	ACS/F606W		4 orbits
	ACS/F814W		14 orbits
	WFC3/F105W	#13495/PI: Lotz	24 orbits
	WFC3/F125W		12 orbits
	WFC3/F140W		10 orbits
	WFC3/F160W		24 orbits
	ACS/F606W,F775W	#17231, PI: Treu	15 orbits
		VLT	
Cluster (HFF-core)	MUSE	Mahler et al. (2018)	3.5, 4, 4, 5 hr
		Subaru	
Cluster ($30' \times 30'$)	Suprime-Cam/B, R_C	Medezinski et al. (2016)	27.58, 26.83
	i', z'		26.31, 26.03 AB
		X-ray	
Cluster	XMM-Newton	#074385010, 385 PI: Kneib	110 ks
	Suzaku	#808008010, Eckert et al. (2016)	75 ks
	Chandra	#23700107, PI: Bogdan	1028 ks
		ALMA	
Cluster	1.1 mm imaging	ALMA#2013.1.00999.S, PI: Bauer	395.6 s
	15 GHz spectral scan	ALMA#2018.1.00035.L, PI: Kohno	95.5 hr
Cluster ($4' \times 6'$)	30 GHz spectral scan	ALMA#2022.1.00073.S, PI: Fujimoto	37.2 hr

3. Image Reduction and Mosaics

This paper focuses on the UNCOVER NIRCam and NIRISS imaging (on the HFF parallel). A full description and public release of photometric and spectroscopic catalogs will be included in subsequent data releases and associated publications.

3.1. Image Reduction

All public JWST NIRCam and NIRISS exposures in the A2744 cluster field were downloaded from the Barbara A. Mikulski Archive for Space Telescopes (MAST). The UNCOVER data sets can be accessed through MAST at doi:10.17909/zn4s-0243, which includes data from the UNCOVER program as well as imaging from the GLASS-ERS (PI: Treu) and DD-2756 (PI: Chen) programs. The data-reduction pipeline Grism redshift and line analysis software for space-based spectroscopy (`Grizli`, version 1.6.0.dev99) was used to process, align, and co-add the exposures. A detailed description of the pipeline is provided in G. Brammer et al. (2024, in preparation).

We start with the MAST `rate.fits` products produced by Stage 1 of the JWST calibration pipeline (v1.8.4) using

Table 4
UNCOVER Data Release Schedule

Data Release	Description	Anticipated Date
DR1/DR2	Imaging mosaics (This paper)	2022 Dec
	Updated gravitational lens model (Furtak et al. 2023c)	2022 Dec
	First-look photometric catalogs (Weaver et al. 2024)	2022 Dec
	Photo-z's and stellar populations (Wang et al. 2024)	2023 Jan
DR3	Photometric catalogs with MegaScience medium bands (Suess et al. 2024)	2024 Apr
DR4	Reduced PRISM spectra (Price et al. 2024)	2024 Aug

calibration set `jwst_0995.pmap`. We derive a correction for the $1/f$ noise (Rauscher 2015) by subtracting the source-masked median image values computed along detector rows and columns. Bright cosmic rays that are not completely mitigated by the Level 1 exposure ramp fit can produce "snowball" residuals (Rigby et al. 2023). Rather than rerunning the ramp fits, we identify likely snowballs as large groups of pixels with the DQ = 4 bit set in the exposure data quality array and grow a conservative mask around them.

Before 2023 May, the flat-field reference files available in the JWST Calibration Reference Data System (CRDS) were determined from calibrations taken on the ground and did not accurately reflect the pixel-to-pixel structure in the in-flight NIRCam data. This is most important in the reddest filters where the background is brightest and therefore where any errors in the multiplicative flat-field correction are largest. We determined NIRCam "sky flat" reference files from on-sky commissioning data from program COM-1063 (PI: Sunnquist) from normalized, source-masked exposures in each of the filter/detector combinations used in the UNCOVER field.[36] The NIRCam long-wavelength CRDS flat-field reference files were updated in 2023 May (`jwst_1084.pmap`) based on in-flight data; however, we use the custom sky flats that were computed in a uniform way for all short- and long-wavelength filter/detector combinations. We apply an additional mask to the exposure data quality arrays to ignore any pixels where the sky flat is outside of the range [0.7, 1.4], essentially removing approximately one out of four images of the same region on the sky due to the dither pattern. Any masked pixels will not contribute to the mosaic and the total effective exposure time at those positions will therefore decrease. On average, 3.7% of pixels are masked for one reason or another in the longest UNCOVER exposures (837 s in F277W), of which $\leqslant$2.8% come from snowball masking. After applying the flat-field calibration, we fit and subtract the additive "wisp" structure in some of the short-wavelength filter/detector combinations (Rigby et al. 2023) using wisp templates derived from the GO-2561 UNCOVER data themselves.[37]

The final step of exposure-level processing is photometric calibration, which was a rapidly evolving topic of discussion at the time the UNCOVER data were taken in late 2022 (Boyer et al. 2022). This discussion was largely resolved with calibrations derived from in-flight data and provided by CRDS `jwst_0989.pmap`. However, we adopt a residual relative correction of 0.94 for the F277W filter in the NIRCam A module based on observations from the PRIMER program (GO-1837, PI: Dunlop) where the same sources were observed in the same filter on both detectors.[38]

After the JWST-specific corrections to the exposures described above, the `grizli` pipeline processing is essentially identical to the procedure adopted earlier for data from the HST (e.g., Kokorev et al. 2022). The most important step of this processing is the image alignment, which is performed in two steps. The first computes shift translations based on the positions of sources identified in each individual exposure; these shifts tend to be small ($\lesssim$0.1 NIRCam pixel) as the pointing control and small offsetting of the telescope are quite precise (Rigby et al. 2023). The absolute alignment is performed by aligning (shift and rotation) the UNCOVER F444W exposures to sources in the ground-based NOAO LegacySurvey DR9 catalog (Dey et al. 2019). We have verified that with this procedure the UNCOVER mosaic is aligned to the absolute frame defined by Gaia DR3 (Gaia Collaboration et al. 2023) at a level of 12 mas (Weaver et al. 2024). We then create a source list from the aligned F444W mosaic to which the exposures in all of the other filters are aligned. The background pedestal level of each exposure is computed with the AstroDrizzle software (Hoffmann et al. 2021), which is then also used to create the final mosaics of each filter drizzled to a common pixel grid with drizzle parameters `pixfrac` = 0.75, `kernel` = `square`.[39] AstroDrizzle produces a "weight" image that has units of inverse variance of the "science" images and is made by propagating the total ERR noise model of each input exposure through the drizzle resampling. The weight map does not account for correlated noise of the finite drizzle pixel resampling (e.g., Casertano et al. 2000). We also compute mosaics of all of the historical Hubble imaging of the A2744 field, drizzled to the same pixel grid and with data sets described by Kokorev et al. (2022) and references therein.

3.2. DR1: Initial Release of NIRCam/NIRISS Mosaics

With this publication, we publicly release fully reduced, multiband mosaics for the first NIRCam cluster and NIRISS parallel imaging with 20 mas pixels in the NIRCam short-wavelength filters and 40 mas pixels in the NIRCam long-wavelength filters and NIRISS imaging. Color images for each mosaic are shown in Figure 6 (NIRCam) and Figure 7 (NIRISS). We also provide reduced HST imaging on the same WCS grids. All of these data products will be hosted initially through Amazon Web Services, linked from the UNCOVER team website,[40] and upon publication uploaded to MAST. This data release is designed to be significantly in advance of the JWST Cycle 2 proposal deadline. Details of this plan can be found in Table 4.

Our team intends to incrementally release higher-level data products associated with these early data (e.g., intracluster-

[36] https://s3.amazonaws.com/grizli-v2/NircamSkyflats/flats.html
[37] https://s3.amazonaws.com/grizli-v2/NircamWisp/index.html
[38] See https://github.com/gbrammer/grizli/pull/143.
[39] Note that `grizli` derives a world coordinate system (WCS) header from the JWST exposure metadata that is compatible with the Simple Imaging Polynomial convention (Shupe et al. 2005) so that the WCS from both JWST and HST exposures can be treated interchangeably.
[40] https://jwst-uncover.github.io/DR1.html

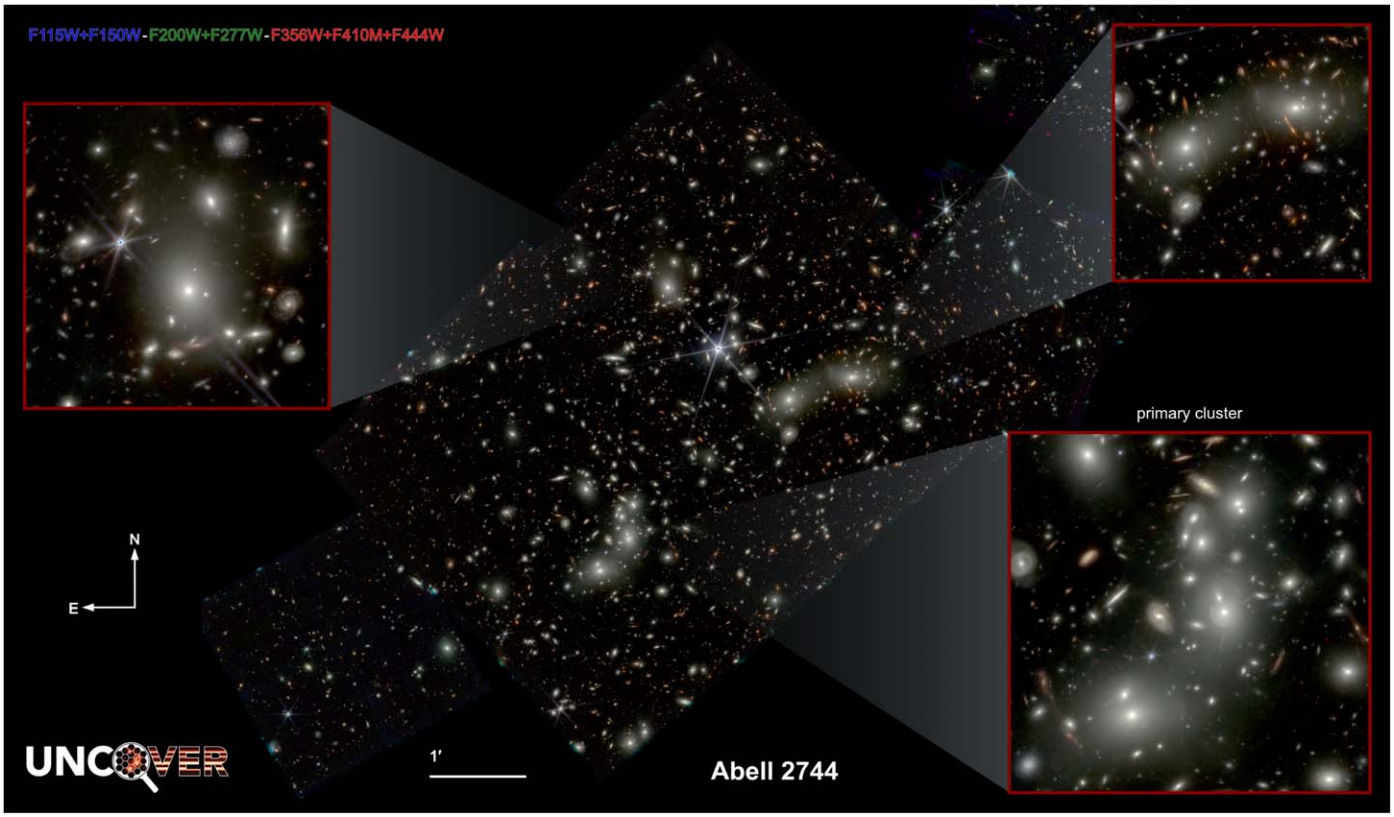

Figure 6. JWST imaging mosaic of A2744 centered on the UNCOVER NIRCam mosaic. We highlight the three observed cluster cores in inset panels; only the Southern primary cluster has been covered by HST imaging in the field. Our imaging of the Northern substructures reveals a multitude of lensed features, that are used to improve the lens modeling in that region (L. Furtak et al. 2024, in preparation). This color image combines all UNCOVER filters and includes other JWST NIRCam/NIRISS imaging in the field including GLASS (Treu et al. 2022) and DDT#2756. A high-resolution version of this color image is available on the UNCOVER website.

light-subtracted mosaics, photometric catalogs and derived properties, and updated gravitational lensing maps) on a short timescale. These data releases will be followed by final catalogs and spectroscopic data releases in the subsequent years.

4. Discussion and Scientific Objectives of the UNCOVER Survey

The JWST UNCOVER survey is designed to address a primary objective of the observatory: detecting and spectroscopically characterizing the properties of the first galaxies while enabling a broad range of scientific explorations. Broadly, our scientific targets fall into four primary categories.

1. *The first galaxies*: The first JWST observations released in 2022 July quickly transformed the field. Early Release Observations in SMACSJ0723.3-7327 (ERO #2736, PI: Pontoppidan; Pontoppidan et al. 2022) and Early Release Science observations from GLASS (#1324, PI: Treu; Treu et al. 2022) and CEERS (#1345, PI: Finkelstein; Bagley et al. 2023) revealed an unexpected abundance of bright galaxies at $10 < z < 17$ (Naidu et al. 2022a; Castellano et al. 2022; Finkelstein et al. 2022; Furtak et al. 2023a; Atek et al. 2023; Donnan et al. 2023; Harikane et al. 2023) and a population of candidate massive ($>10^{10} M_{\odot}$) galaxies at $7 < z < 10$ (Labbé et al. 2023), which may or may not be in tension with galaxy formation model predictions (Boylan-Kolchin 2023; Ferrara et al. 2023; Mason et al. 2023; Nath et al. 2023). The NIRCam imaging from UNCOVER extends these early efforts by providing deep 3.7 hr (∼30 AB F200W) imaging over a large area with gravitational lensing ($\mu > 2$ over >17 arcmin^2), ideally suited to improve statistics of galaxies at $z > 10$ (see Table 2). The ultradeep 2.7–20 hr $R \sim 100$ PRISM spectra can provide spectroscopic continuum redshifts of any JWST-selected galaxy to 29 AB, unbiased with respect to the presence of emission lines or targeting, providing the first comprehensive test of the photometric selection at these redshifts. The early UNCOVER spectra revealed a number of stunning examples of these incredibly distant galaxies (Fujimoto et al. 2023b; Wang et al. 2023).
2. *The reionization era*: Understanding how and when galaxies irradiated their environment and reionized the surrounding neutral gas is a key outstanding question. Determining the contribution of galaxies to reionization requires a full accounting of the faintest galaxies that dominate the integrated UV light, the rate at which they produce ionizing photons, and the fraction of photons that escape. UNCOVER imaging will securely detect galaxies to $M_{\rm UV} \sim -14$ and should settle the issue of the potential turnover (e.g., Bouwens et al. 2022b), directly measuring 85% of the reionizing UV radiation (e.g., Livermore et al. 2017, and references therein). The 3× spatial resolution improvement of NIRCam versus HST/WFC3 better constrains the size distribution of the galaxy population, further mitigating systematic sources of error. Ultradeep PRISM spectra enable the study of ionizing spectra of the faintest galaxies (down to $M_{\rm UV} \sim -15$; Atek et al. 2024).

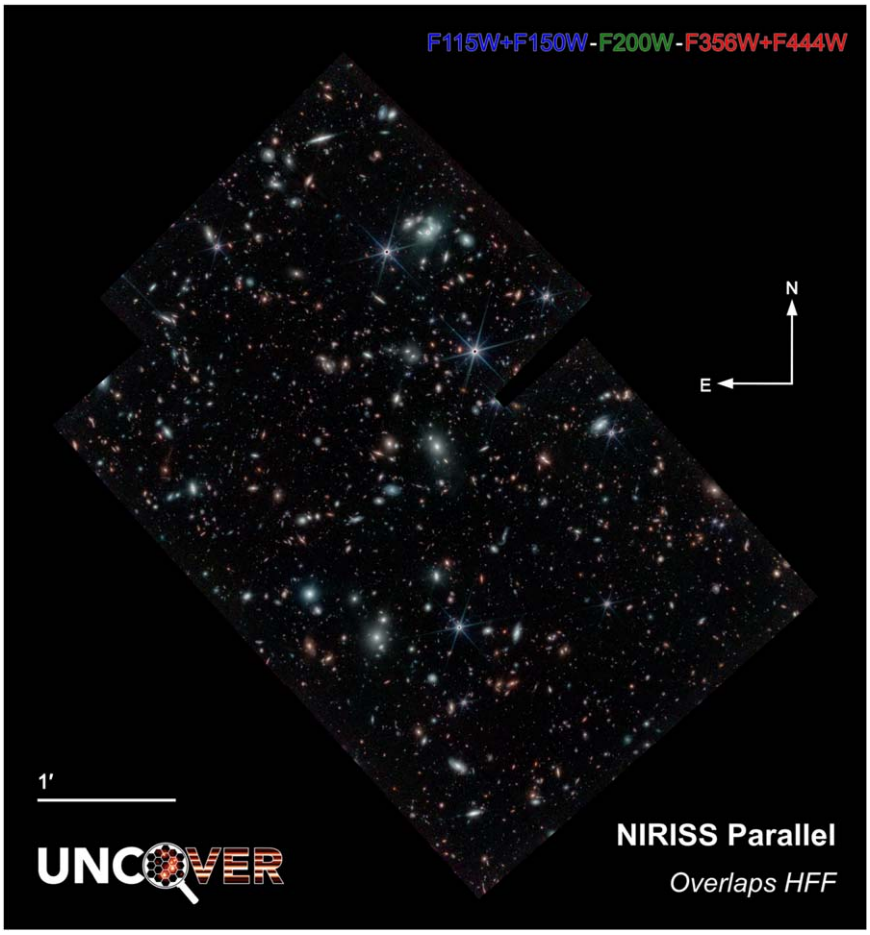

Figure 7. Color image of the UNCOVER NIRISS parallel, which overlaps with the HFF parallel.

Of the expected ∼1500 galaxies at $z = 6$–7, we estimate about ∼40 will have intrinsic UV magnitudes of $M_{\rm UV} > -16$ but still be bright enough (<28 AB) to get high-quality spectra. For these galaxies we will observe the full complement of strong optical lines ([O II], [O III], Hβ, Hα, [N II], [S II], with Hα and [N II] marginally resolved at $R \sim 300$ at $\sim 5\,\mu$m), to study interstellar medium properties, ages, metallicities, and ionization mechanisms. The combination of imaging and spectra has the potential to be a quantum leap in studies of reionization-era galaxies.

3. *The emergence of dusty galaxies:* The fraction of star formation missed due to dust at $z > 4$ and at low luminosities remains unclear. ALMA has discovered dusty galaxies with relatively low masses and star formation rates already at $z > 5$ (e.g., Wang et al. 2019; Williams et al. 2019; Yamaguchi et al. 2019; Fudamoto et al. 2021; Dayal et al. 2022; Algera et al. 2023), suggesting that dust-obscured star formation may be more prominent than was expected. These highly obscured extreme starbursts known to exist may represent only the tip of the iceberg. Detection of starlight from "HST-dark" galaxies was expected in deep JWST imaging; early imaging has indeed revealed a substantial population (Barrufet et al. 2023; Nelson et al. 2023; Pérez-González et al. 2023; Price et al. 2023) of extreme red, dusty galaxies extending to $z \sim 7$–8. UNCOVER will place strong constraints at the lowest masses and the highest redshifts, complementary to the JWST wide-field programs, e.g., COSMOS-Web (GO #1727, PI: Kartaltepe and Casey; Casey et al. 2023) and PANORAMIC (GO #2514, PIs: Williams and Oesch), capable of finding massive obscured galaxies over larger volumes. The ability to detect any highly obscured $M_\star > 10^9 M_\odot$ galaxy to $z = 9$ with NIRCam and test photometric stellar population inferences with NIRSpec spectroscopy will further expand our census of star formation.
4. *The epoch of quenching:* Quenching of star formation is a complex phenomenon, with different processes dominating over a range of times, mass scales, and environments. The earliest massive quiescent galaxies have been spectroscopically confirmed to redshift $z \sim 4$ (e.g., Glazebrook et al. 2017; Schreiber et al. 2018; Forrest et al. 2020). However, this is entirely limited by detection: quiescent galaxies almost certainly exist to lower masses and higher redshift beyond the capabilities of HST and ground-based spectroscopy. The first JWST imaging has already provided spectacular candidates of massive, quiescent galaxies to redshift ∼5 (Carnall et al. 2022). UNCOVER NIRCam imaging will extend the search for quiescent galaxies to unprecedented low mass and high redshift, i.e., $<10^9 M_\odot$ to $z = 9$. Marchesini et al. (2023) demonstrated the presence of $10^{10} M_\odot$ quiescent galaxies to $z \sim 2.5$ with early NIRISS spectra. The UNCOVER NIRSpec/PRISM spectroscopy will be able to push this to even lower masses and higher redshifts due

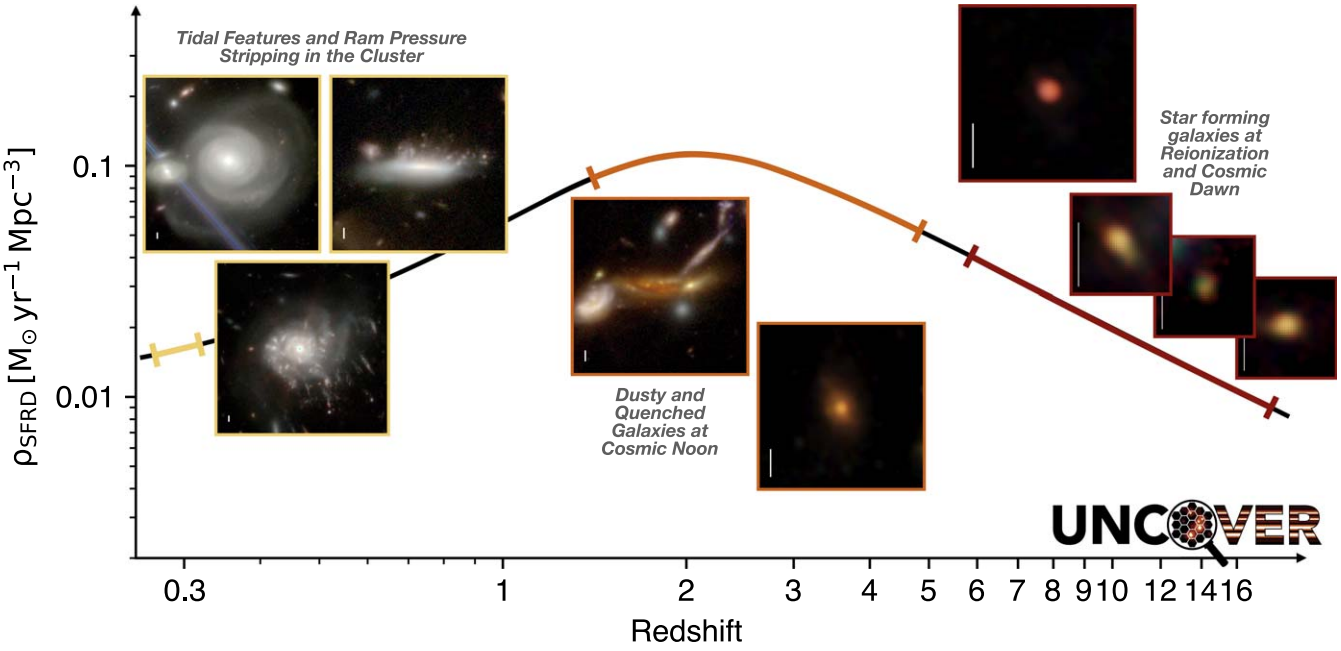

Figure 8. UNCOVER imaging reveals spectacular views of a vast array of galaxies across cosmic time, shown here as drawn from the history of the cosmic star formation rate density from Casey et al. (2018). These galaxies span foreground galaxies within the A2744 cluster, to red and/or remarkably resolved lensed systems at Cosmic Noon (submillimeter galaxy A2744-ID02 from González-López et al. 2017 and a quiescent galaxy candidate), and back into the most extreme—and therefore uncertain—epochs to the time of the first galaxies (GLASSz8-1 from Roberts-Borsani et al. 2022 and triply lensed JD1 from Zitrin et al. 2014). White scale bars indicate $0\farcs5$ on all postage stamps.

to the improved depth and wavelength coverage to $\sim$5.3 μm to confirm the quiescence through the absence of emission lines and strong Balmer breaks (e.g., Setton et al. 2024). Beyond identification and counting, the PRISM spectroscopy will also be deep enough to further constrain stellar populations to $F444W \lesssim 27.5$ AB from the stellar continuum.

5. *The unknown unknowns:* Perhaps the most exciting legacy of deep fields like UNCOVER is the potential to discover objects that we have not yet imagined or identify predicted objects that we never hoped to detect in addition to offering possible constraints on the non-cold-dark-matter nature of dark matter (e.g., Dayal et al. 2015). The advance in sensitivity, wavelength coverage, and spectral resolution is so large that we will certainly run into surprises. The UNCOVER treasury program ensures a comprehensive exploration of ultradeep parameter space with public imaging and spectroscopy released early in JWST's mission. An extraordinary example of this fruitful discovery space has been the abundance of actively accreting black holes that have been discovered and studied within the UNCOVER imaging (e.g., Furtak et al. 2023b; Greene et al. 2024) and spectroscopy (e.g., Goulding et al. 2023; Kokorev et al. 2023; Furtak et al. 2024).

The astronomical community has only begun to scratch the surface of possible JWST observations of the distant Universe. This paper aims to present a basic description of the UNCOVER Treasury program to optimize community use of early data products, prepare for Cycle 2 JWST proposals targeting objects in and behind the A2744 cluster, and anticipate the use of the scheduled NIRSpec/PRISM follow-up. These studies are likely to range from detailed analyses of previously known sources to exciting JWST discoveries. We conclude this paper by highlighting the broad range of UNCOVER scientific targets in Figure 8. Individual objects are plotted against the backdrop of dust-rich and dust-poor models for the evolution of the star formation rate density from Casey et al. (2018).

Even in Cycle 1, the community had access to a wide range of exciting JWST data sets probing the distant Universe. Some of these programs will enable detailed high-resolution studies of extremely lensed sources, as in TEMPLATES (ERS #1355, PIs: Rigby and Viera). The JWST-GLASS program (ERS #1324, PI: Treu) provides an in-depth and multipronged view of reionization in the A2744 cluster (Treu et al. 2022). The CEERS program provides a range of relatively shallow imaging and spectroscopy across the well-studied CANDELS Extended Groth Strip field (ERS #1324, PI: Finkelstein; Finkelstein et al. 2023). Other GO programs will expand imaging footprints: PRIMER (GO #1837, PI: Dunlop) will map nearly 700 sq. arcmin with 10 NIRCam and MIRI filters (236 sq. arcmin in MIRI) and COSMOS-Web will map an incredible 0.6 square degrees in NIRCam and 0.2 square degrees in MIRI with a smaller number of filters (GO #1727, PIs: Kartaltepe and Casey; Casey et al. 2023). Finally, the pure parallel program PANORAMIC (GO #2514, PIs: Williams and Oesch) is planned to provide multiband NIRCam imaging of spatially uncorrelated pointings covering up to 0.4 square degrees with a range of depths.

The UNCOVER program explores a unique parameter space; reaching within a magnitude of the GTO ultradeep field but boosted by gravitational lensing and with no proprietary access. Although this is just the first of several planned public data releases, our team looks forward to seeing what the community will uncover from this and all other JWST treasure troves.

Acknowledgments

R.B. acknowledges support from the Research Corporation for Scientific Advancement (RCSA) Cottrell Scholar Award ID No. 27587. Cloud-based data processing and file storage for this work is provided by the AWS Cloud Credits for Research program. This work is based in part on observations made with the NASA/ESA/CSA James Webb Space Telescope. The data were obtained from the Mikulski Archive for Space Telescopes at the Space Telescope Science Institute, which is operated by the Association of Universities for Research in Astronomy, Inc., under NASA contract NAS 5-03127 for JWST. These observations are associated with JWST Cycle 1 GO programs #2561, JWST-ERS-1324, and JWST-DD-2756. Support for program JWST-GO-2561 was provided by NASA through a grant from the Space Telescope Science Institute, which is operated by the Associations of Universities for Research in Astronomy, Incorporated, under NASA contract NAS 5-26555. This research is based on observations made with the NASA/ESA Hubble Space Telescope obtained from the Space Telescope Science Institute, which is operated by the Association of Universities for Research in Astronomy, Inc., under NASA contract NAS 5-26555. These observations are associated with programs HST-GO-11689, HST-GO-13386, HST-GO/DD-13495, HST-GO-13389, HST-GO-15117, and HST-GO/DD-17231. The Cosmic Dawn Center is funded by the Danish National Research Foundation (DNRF) under grant No. 140. This research was supported in part by the University of Pittsburgh Center for Research Computing, RRID: SCR_022735, through the resources provided. Specifically, this work used the H2P cluster, which is supported by NSF award number OAC-2117681. L.F. and A.Z. acknowledge support by grant No. 2020750 from the United States-Israel Binational Science Foundation (BSF) and grant No. 2109066 from the United States National Science Foundation (NSF) and by the Ministry of Science & Technology, Israel. P.D. acknowledges support from the NWO grant 016.VIDI.189.162 ("ODIN") and from the European Commission's and University of Groningen's CO-FUND Rosalind Franklin program. H.A. acknowledges support from CNES (Centre National d'Etudes Spatiales). R.S. acknowledges an STFC Ernest Rutherford Fellowship (ST/S004831/1). M.S. acknowledges support from the CIDEGENT/2021/059 grant, from project PID2019-109592GB-I00/AEI/10.13039/501100011033 from the Spanish Ministerio de Ciencia e Innovación - Agencia Estatal de Investigación, and from Proyecto ASFAE/2022/025 del Ministerio de Ciencia y Innovación en el marco del Plan de Recuperación, Transformación y Resiliencia del Gobierno de España. The work of CCW is supported by NOIRLab, which is managed by the Association of Universities for Research in Astronomy (AURA) under a cooperative agreement with the National Science Foundation.

Facilities: JWST (NIRCam, NIRSpec, and NIRISS), HST (ACS and WFC3).

Software: astropy (Astropy Collaboration et al. 2013, 2018, 2022), Bagpipes (Carnall et al. 2018), Grizli Brammer & Matharu (2021), Prospector (Johnson et al. 2021), DrizzlePac (Hoffmann et al. 2021).

ORCID iDs

Rachel Bezanson https://orcid.org/0000-0001-5063-8254
Ivo Labbe https://orcid.org/0000-0002-2057-5376
Katherine E. Whitaker https://orcid.org/0000-0001-7160-3632
Joel Leja https://orcid.org/0000-0001-6755-1315
Sedona H. Price https://orcid.org/0000-0002-0108-4176
Marijn Franx https://orcid.org/0000-0002-8871-3026
Gabriel Brammer https://orcid.org/0000-0003-2680-005X
Danilo Marchesini https://orcid.org/0000-0001-9002-3502
Adi Zitrin https://orcid.org/0000-0002-0350-4488
Bingjie Wang (王冰洁) https://orcid.org/0000-0001-9269-5046
John R. Weaver https://orcid.org/0000-0003-1614-196X
Lukas J. Furtak https://orcid.org/0000-0001-6278-032X
Hakim Atek https://orcid.org/0000-0002-7570-0824
Dan Coe https://orcid.org/0000-0001-7410-7669
Sam E. Cutler https://orcid.org/0000-0002-7031-2865
Pratika Dayal https://orcid.org/0000-0001-8460-1564
Pieter van Dokkum https://orcid.org/0000-0002-8282-9888
Robert Feldmann https://orcid.org/0000-0002-1109-1919
Natascha M. Förster Schreiber https://orcid.org/0000-0003-4264-3381
Seiji Fujimoto https://orcid.org/0000-0001-7201-5066
Marla Geha https://orcid.org/0000-0002-7007-9725
Karl Glazebrook https://orcid.org/0000-0002-3254-9044
Anna de Graaff https://orcid.org/0000-0002-2380-9801
Jenny E. Greene https://orcid.org/0000-0002-5612-3427
Stéphanie Juneau https://orcid.org/0000-0002-0000-2394
Susan Kassin https://orcid.org/0000-0002-3838-8093
Mariska Kriek https://orcid.org/0000-0002-7613-9872
Gourav Khullar https://orcid.org/0000-0002-3475-7648
Michael Maseda https://orcid.org/0000-0003-0695-4414
Lamiya A. Mowla https://orcid.org/0000-0002-8530-9765
Adam Muzzin https://orcid.org/0000-0002-9330-9108
Themiya Nanayakkara https://orcid.org/0000-0003-2804-0648
Erica J. Nelson https://orcid.org/0000-0002-7524-374X
Pascal A. Oesch https://orcid.org/0000-0001-5851-6649
Camilla Pacifici https://orcid.org/0000-0003-4196-0617
Richard Pan https://orcid.org/0000-0002-9651-5716
Casey Papovich https://orcid.org/0000-0001-7503-8482
David J. Setton https://orcid.org/0000-0003-4075-7393
Alice E. Shapley https://orcid.org/0000-0003-3509-4855
Renske Smit https://orcid.org/0000-0001-8034-7802
Mauro Stefanon https://orcid.org/0000-0001-7768-5309
Edward N. Taylor https://orcid.org/0000-0002-5522-9107
Christina C. Williams https://orcid.org/0000-0003-2919-7495

References

Adams, N. J., Conselice, C. J., Ferreira, L., et al. 2023, MNRAS, 518, 4755
Algera, H. S. B., Inami, H., Oesch, P. A., et al. 2023, MNRAS, 518, 6142
Astropy Collaboration, Price-Whelan, A. M., Lim, P. L., et al. 2022, ApJ, 935, 167
Astropy Collaboration, Price-Whelan, A. M., Sipőcz, B. M., et al. 2018, AJ, 156, 123
Astropy Collaboration, Robitaille, T. P., Tollerud, E. J., et al. 2013, A&A, 558, A33
Atek, H., Labbé, I., Furtak, L. J., et al. 2024, Natur, 626, 975
Atek, H., Richard, J., Kneib, J.-P., & Schaerer, D. 2018, MNRAS, 479, 5184
Atek, H., Shuntov, M., Furtak, L. J., et al. 2023, MNRAS, 519, 1201
Bagley, M. B., Finkelstein, S. L., Koekemoer, A. M., et al. 2023, ApJL, 946, L12
Bagley, M. B., Pirzkal, N., Finkelstein, S. L., et al. 2024, ApJL, 965, L6
Barrufet, L., Oesch, P. A., Weibel, A., et al. 2023, MNRAS, 522, 449
Bhatawdekar, R., Conselice, C. J., Margalef-Bentabol, B., & Duncan, K. 2019, MNRAS, 486, 3805

Böker, T., Beck, T. L., Birkmann, S. M., et al. 2023, PASP, 135, 038001
Bouwens, R. J., Illingworth, G., Ellis, R. S., Oesch, P., & Stefanon, M. 2022b, ApJ, 940, 55
Bouwens, R. J., Illingworth, G., Ellis, R. S., et al. 2022a, ApJ, 931, 81
Bouwens, R. J., Oesch, P. A., Stefanon, M., et al. 2021, AJ, 162, 47
Boyer, M. L., Anderson, J., Gennaro, M., et al. 2022, RNAAS, 6, 191
Boylan-Kolchin, M. 2023, NatAs, 7, 731
Brammer, G., & Matharu, J. 2021, gbrammer/grizli: Release 2021, 1.3.2, Zenodo, doi:10.5281/zenodo.5012699
Carnall, A. C., McLure, R. J., Dunlop, J. S., & Davé, R. 2018, MNRAS, 480, 4379
Carnall, A. C., McLure, R. J., Dunlop, J. S., et al. 2022, ApJ, 929, 131
Casertano, S., de Mello, D., Dickinson, M., et al. 2000, AJ, 120, 2747
Casey, C. M., Kartaltepe, J. S., Drakos, N. E., et al. 2023, ApJ, 954, 31
Casey, C. M., Zavala, J. A., Spilker, J., et al. 2018, ApJ, 862, 77
Castellano, M., Fontana, A., Treu, T., et al. 2022, ApJL, 938, L15
Coe, D., Zitrin, A., Carrasco, M., et al. 2013, ApJ, 762, 32
Dayal, P., & Ferrara, A. 2018, PhR, 780, 1
Dayal, P., Ferrara, A., Dunlop, J. S., & Pacucci, F. 2014, MNRAS, 445, 2545
Dayal, P., Ferrara, A., Sommovigo, L., et al. 2022, MNRAS, 512, 989
Dayal, P., Mesinger, A., & Pacucci, F. 2015, ApJ, 806, 67
Dey, A., Schlegel, D. J., Lang, D., et al. 2019, AJ, 157, 168
Diego, J. M., Broadhurst, T., Wong, J., et al. 2016, MNRAS, 459, 3447
Donnan, C. T., McLeod, D. J., Dunlop, J. S., et al. 2023, MNRAS, 518, 6011
Doyon, R., Hutchings, J. B., Beaulieu, M., et al. 2012, Proc. SPIE, 8442, 84422R
Duncan, K., Conselice, C. J., Mortlock, A., et al. 2014, MNRAS, 444, 2960
Eckert, D., Jauzac, M., Vazza, F., et al. 2016, MNRAS, 461, 1302
Ferrara, A., Pallottini, A., & Dayal, P. 2023, MNRAS, 522, 3986
Finkelstein, S. L., Bagley, M. B., Ferguson, H. C., et al. 2023, ApJL, 946, L13
Finkelstein, S. L., Bagley, M. B., Haro, P. A., et al. 2022, ApJL, 940, L55
Finkelstein, S. L., Ryan, R. E. J., Papovich, C., et al. 2015, ApJ, 810, 71
Forrest, B., Annunziatella, M., Wilson, G., et al. 2020, ApJL, 890, L1
Fudamoto, Y., Oesch, P. A., Schouws, S., et al. 2021, Natur, 597, 489
Fujimoto, S., Bezanson, R., Labbe, I., et al. 2023a, arXiv:2309.07834
Fujimoto, S., Wang, B., Weaver, J., et al. 2023b, arXiv:2308.11609
Furtak, L. J., Atek, H., Lehnert, M. D., Chevallard, J., & Charlot, S. 2021, MNRAS, 501, 1568
Furtak, L. J., Labbé, I., Zitrin, A., et al. 2024, Natur, 628, 57
Furtak, L. J., Shuntov, M., Atek, H., et al. 2023a, MNRAS, 519, 3064
Furtak, L. J., Zitrin, A., Plat, A., et al. 2023b, ApJ, 952, 142
Furtak, L. J., Zitrin, A., Weaver, J. R., et al. 2023c, MNRAS, 523, 4568
Gaia Collaboration, Vallenari, A., Brown, A. G. A., et al. 2023, A&A, 674, A1
Glazebrook, K., Schreiber, C., Labbé, I., et al. 2017, Natur, 544, 71
González-López, J., Bauer, F. E., Romero-Cañizales, C., et al. 2017, A&A, 597, A41
Goulding, A. D., Greene, J. E., Setton, D. J., et al. 2023, ApJL, 955, L24
Grazian, A., Fontana, A., Santini, P., et al. 2015, A&A, 575, A96
Greene, J. E., Labbe, I., Goulding, A. D., et al. 2024, ApJ, 964, 39
Harikane, Y., Ouchi, M., Oguri, M., et al. 2023, ApJS, 265, 5
Hoffmann, S. L., Mack, J., Avila, R., et al. 2021, AAS Meeting, 238, 216.02
Ishigaki, M., Kawamata, R., Ouchi, M., et al. 2018, ApJ, 854, 73
Jakobsen, P., Ferruit, P., Alves de Oliveira, C., et al. 2022, A&A, 661, A80
Jauzac, M., Richard, J., Jullo, E., et al. 2015, MNRAS, 452, 1437
Johnson, B. D., Leja, J., Conroy, C., & Speagle, J. S. 2021, ApJS, 254, 22
Kauffmann, O. B., Ilbert, O., Weaver, J. R., et al. 2022, A&A, 667, A65
Kauffmann, O. B., Le Fèvre, O., Ilbert, O., et al. 2020, A&A, 640, A67
Kawamata, R., Oguri, M., Ishigaki, M., Shimasaku, K., & Ouchi, M. 2016, ApJ, 819, 114
Kelly, P. L., Rodney, S. A., Treu, T., et al. 2015, Sci, 347, 1123
Kikuchihara, S., Ouchi, M., Ono, Y., et al. 2020, ApJ, 893, 60
Kohno, K. 2019, ALMA2019: Science Results and Cross-Facility Synergies (Garching bei München: ESO), 64, http://www.eso.org/sci/meetings/2019/ALMA2019Cagliari.html
Kokorev, V., Brammer, G., Fujimoto, S., et al. 2022, ApJS, 263, 38
Kokorev, V., Fujimoto, S., Labbe, I., et al. 2023, ApJL, 957, L7
Labbé, I., Oesch, P. A., Bouwens, R. J., et al. 2013, ApJL, 777, L19
Labbé, I., van Dokkum, P., Nelson, E., et al. 2023, Natur, 616, 266
Leja, J., Garg, P., Johnson, B. D., et al. 2021, JWST Proposal. Cycle 1, 2354
Leja, J., Speagle, J. S., Johnson, B. D., et al. 2020, ApJ, 893, 111
Livermore, R. C., Finkelstein, S. L., & Lotz, J. M. 2017, ApJ, 835, 113
Lotz, J. M., Koekemoer, A., Coe, D., et al. 2017, ApJ, 837, 97
Madau, P., & Dickinson, M. 2014, ARA&A, 52, 415
Mahler, G., Richard, J., Clément, B., et al. 2018, MNRAS, 473, 663
Marchesini, D., Brammer, G., Morishita, T., et al. 2023, ApJL, 942, L25
Mason, C. A., Trenti, M., & Treu, T. 2015, ApJ, 813, 21
Mason, C. A., Trenti, M., & Treu, T. 2023, MNRAS, 521, 497
Medezinski, E., Umetsu, K., Okabe, N., et al. 2016, ApJ, 817, 24
Merten, J., Coe, D., Dupke, R., et al. 2011, MNRAS, 417, 333
Naidu, R. P., Oesch, P. A., Dokkum, P. v., et al. 2022a, ApJL, 940, L14
Naidu, R. P., Oesch, P. A., Setton, D. J., et al. 2022b, arXiv:2208.02794
Nath, B. B., Vasiliev, E. O., Drozdov, S. A., & Shchekinov, Y. A. 2023, MNRAS, 521, 662
Nelson, E. J., Suess, K. A., Bezanson, R., et al. 2023, ApJL, 948, L18
Oesch, P. A., Bouwens, R. J., Illingworth, G. D., Labbé, I., & Stefanon, M. 2018, ApJ, 855, 105
Oesch, P. A., Brammer, G., van Dokkum, P. G., et al. 2016, ApJ, 819, 129
Paris, D., Merlin, E., Fontana, A., et al. 2023, ApJ, 952, 20
Pérez-González, P. G., Barro, G., Annunziatella, M., et al. 2023, ApJL, 946, L16
Pontoppidan, K. M., Barrientes, J., Blome, C., et al. 2022, ApJL, 936, L14
Price, S. H., Bezanson, R., Labbe, I., et al. 2024, arXiv:2408.03920
Price, S. H., Suess, K. A., Williams, C. C., et al. 2023, arXiv:2310.02500
Rauscher, B. J. 2015, PASP, 127, 1144
Richard, J., Jauzac, M., Limousin, M., et al. 2014, MNRAS, 444, 268
Rieke, M. J., Baum, S. A., Beichman, C. A., et al. 2003, Proc. SPIE, 4850, 478
Rieke, M. J., Kelly, D., & Horner, S. 2005, Proc. SPIE, 5904, 1
Rieke, M. J., Kelly, D. M., Misselt, K., et al. 2023, PASP, 135, 028001
Rigby, J., Perrin, M., McElwain, M., et al. 2023, PASP, 135, 048001
Roberts-Borsani, G., Morishita, T., Treu, T., et al. 2022, ApJL, 938, L13
Roberts-Borsani, G., Treu, T., Mason, C., et al. 2021, ApJ, 910, 86
Schreiber, C., Glazebrook, K., Nanayakkara, T., et al. 2018, A&A, 618, A85
Setton, D. J., Khullar, G., Miller, T. B., et al. 2024, arXiv:2402.05664
Shupe, D. L., Moshir, M., Li, J., et al. 2005, in ASP Conf. Ser. 347, Astronomical Data Analysis Software and Systems XIV, ed. P. Shopbell, M. Britton, & R. Ebert (San Francisco, CA: ASP), 491
Smit, R., Bouwens, R. J., Labbé, I., et al. 2014, ApJ, 784, 58
Song, M., Finkelstein, S. L., Ashby, M. L. N., et al. 2016, ApJ, 825, 5
Stark, D. 2012, Natur, 489, 370
Stefanon, M., Bouwens, R. J., Illingworth, G. D., et al. 2022, ApJ, 935, 94
Stefanon, M., Bouwens, R. J., Labbé, I., et al. 2021, ApJ, 922, 29
Steinhardt, C. L., Jauzac, M., Acebron, A., et al. 2020, ApJS, 247, 64
Suess, K. A., Weaver, J. R., Price, S. H., et al. 2024, arXiv:2404.13132
Treu, T., Roberts-Borsani, G., Bradac, M., et al. 2022, ApJ, 935, 110
Ucci, G., Dayal, P., Hutter, A., et al. 2021, MNRAS, 506, 202
Wang, B., Fujimoto, S., Labbé, I., et al. 2023, ApJL, 957, L34
Wang, B., Leja, J., Labbé, I., et al. 2024, ApJS, 270, 12
Wang, T., Schreiber, C., Elbaz, D., et al. 2019, Natur, 572, 211
Wang, X., Hoag, A., Huang, K. H., et al. 2015, ApJ, 811, 29
Weaver, J. R., Cutler, S. E., Pan, R., et al. 2024, ApJS, 270, 7
Williams, C. C., Curtis-Lake, E., Hainline, K. N., et al. 2018, ApJS, 236, 33
Williams, C. C., Labbe, I., Spilker, J., et al. 2019, ApJ, 884, 154
Williams, H., Kelly, P. L., Chen, W., et al. 2023, Sci, 380, 416
Windhorst, R. A., Cohen, S. H., Jansen, R. A., et al. 2023, AJ, 165, 13
Yamaguchi, Y., Kohno, K., Hatsukade, B., et al. 2019, ApJ, 878, 73
Zavala, J. A., Buat, V., Casey, C. M., et al. 2023, ApJL, 943, L9
Zitrin, A., Zheng, W., Broadhurst, T., et al. 2014, ApJL, 793, L12